Evaluation of flame area based on detailed chemistry DNS of premixed turbulent hydrogen-air flames in different regimes of combustion

M. Klein[1,*], A. Herbert[1], H. Kosaka[2], B. Böhm[2], A. Dreizler[2], N. Chakraborty[3], V. Papapostolou[3], H. G. Im[4] and J. Hasslberger[1]

[1]Bundeswehr University Munich, Department of Aerospace Engineering, Neubiberg, Germany

[2]Institute of Reactive Flows and Diagnostics, Technische Universität Darmstadt, Germany

[3]School of Engineering, Newcastle University, Newcastle-Upon-Tyne, NE1 7RU, UK

[4]Clean Combustion Research Center, KAUST, Saudi Arabia

*Corresponding author: markus.klein@unibw.de

ABSTRACT

Precise evaluation of flame surface area plays a pivotal role in the fundamental understanding and accurate modelling of turbulent premixed flames. This necessity is reflected in the requirement for the instantaneous flame area evaluation of the turbulent burning velocity (by making use of Damköhler's first hypothesis). Moreover, the information regarding flame area is required in the context of flame surface density based modelling, and for determining the wrinkling factor or estimating the efficiency function. Usually flame surface areas in experiments and Direct Numerical Simulation (DNS) analyses are evaluated differently and the present analysis aims at comparing these approaches by making use of a detailed chemistry DNS database of turbulent, statistically planar flames. It has been found that the flame surface area evaluation is sensitive to the choice of scalar quantity and the isosurface level, and this holds particularly true for two-dimensional evaluations. The conditions, which provide a satisfactory agreement between experimental and numerical approaches in the flame area evaluation, have been identified by a detailed comparative analysis of the usual postprocessing techniques.

Keywords: Detailed chemistry Direct Numerical Simulation, Damköhler's first hypothesis, Turbulent flame area, Experimental postprocessing, Flame surface density;

1. INTRODUCTION

Modelling the turbulent burning velocity S_T in premixed turbulent combustion is of fundamental importance, for an overview of different approaches see [1,2]. Nevertheless, determination of a universal model for this quantity is still a subject of active research [3,4]. The turbulent burning velocity is defined as:

$$S_T = \frac{1}{\rho_0 A_L} \int_V \dot{w} dV. \tag{1}$$

Here $\dot{w}$ is the reaction rate of the reaction progress variable, ρ_0 is the unburned gas density and A_L is the projected flame surface in the direction of mean flame propagation. Throughout this text adiabatic combustion is assumed. The sum of mean/filtered reaction rate and molecular diffusion of a normalised reaction progress variable c (assuming the value 0 in the fresh gas and 1 in the fully burned products) can be written as:

$$\overline{\dot{w} + \nabla \cdot (\rho D_c \nabla c)} = \overline{(\rho S_d)}_s \Sigma_{gen} \tag{2}$$

where D_c is the diffusivity, $S_d = |\nabla c|^{-1}(Dc/Dt)$ is the displacement speed of a given $c = c^*$ isosurface, $\Sigma_{gen} = \overline{|\nabla c|}$ is the generalised flame surface density (FSD) [5] and $\overline{(Q)}_s = \overline{Q|\nabla c|}/\overline{|\nabla c|}$ is the surface-weighted value of a general variable Q with the overbar denoting a Reynolds averaging or LES filtering operation, as appropriate. If not stated otherwise, c will be considered based on non-dimensional temperature $c_T = (\hat{T} - T_0)/(T_{ad} - T_0)$ with $\hat{T}, T_0$ and T_{ad} being the dimensional temperature, unburned gas temperature and adiabatic flame temperature, respectively. It is noted that the molecular (filtered molecular) diffusion term vanishes upon integration according to divergence theorem,

$$\int_V \nabla.(\rho D_c \nabla c) dV = \int_V \overline{\nabla.(\rho D_c \nabla c)} dV = 0 \tag{3}$$

and that Eq. (1) can alternatively be written in terms of averaging/filtering

$$S_T = \frac{1}{\rho_0 A_L} \int_V \bar{\dot{w}} dV. \tag{4}$$

Furthermore, the turbulent flame area can be evaluated by integrating the FSD [6]

$$A_T = \int_V \Sigma_{gen} dV. \tag{5}$$

Combining Eqns. (1)-(5) one obtains:

$$S_T A_L = \frac{\int_V \dot{w} dV}{\rho_0} = \frac{\int_V \overline{(\rho S_d)}_s \Sigma_{gen} dV}{\rho_0 \int_V \Sigma_{gen} dV} \int_V \Sigma_{gen} dV = \frac{\int_V \overline{(\rho S_d)}_s \Sigma_{gen} dV}{\rho_0 \int_V \Sigma_{gen} dV} A_T \tag{6}$$

and with the definition of a modified flame speed:

$$S_L' = \frac{\int_V \overline{(\rho S_d)}_s \Sigma_{gen} dV}{\rho_0 \int_V \Sigma_{gen} dV}, \tag{7}$$

that accounts for volume-integrated FSD-weighted stretch rate dependence of the local displacement speed divided by ρ_0, one can finally write [7]:

$$\frac{S_T}{S_L'} = \frac{A_T}{A_L} \tag{8}$$

Eq. (7) can be rewritten in the following manner

$$S_L' = \frac{\int_V \overline{(\rho S_d)}_s \Sigma_{gen} dV}{\rho_0 \int_V \Sigma_{gen} dV} = \frac{\int_V \bar{\dot{w}} dV}{\rho_0 A_T} = \frac{\int_A \int \dot{w} dn \, dA}{\rho_0 A_T} = \frac{\int_A S_c dA}{A_T} \tag{9}$$

where $S_c = \rho_0^{-1} \int \dot{w} dn$ is the consumption speed. The above expression indicates that the modified flame speed S_L' can be interpreted as the area-weighted mean consumption speed.

Surface averaged, density weighted displacement speed $\overline{(\rho S_d)}_s$ is often approximated as $\overline{(\rho S_d)}_s = \rho_0 S_L^0$ [5,8], where S_L^0 is the unstretched laminar flame speed. This reduces S_L' to S_L^0 and Eq. (8) to Damköhler's first hypothesis:

$$\frac{S_T}{S_L^0} = \frac{A_T}{A_L} \tag{10}$$

The range of validity of Eq. (10) has been recently discussed by means of DNS [9,10] and experiment [11]. Nivarti and Cant [9] found that Damköhler's first hypothesis retains its validity up to large values of turbulence intensity and this has been confirmed by a recent study of Ahmed et al. [10]. In the context of constant density flows, Sabelnikov et al. [12] reported that turbulent burning velocity is mainly controlled by the reaction surface area even for high Karlovitz numbers. Gülder [11] argues that there is a growing body of experimental evidence not supporting Eq. (10). Chakraborty et al. [7] report that Eq. (10) remains valid for statistically planar unity Lewis number flames but can become inaccurate for flames with a sufficiently high non-zero mean curvature. It is worth noting that in contrast to Eq. (10), $S_T/S_L' = A_T/A_L$ is an exact equation provided A_T and S_L' represent the quantities, defined by Eqs. (5) and (7).

However, 3D experimental evaluation of the quantities A_T and S_L' remains challenging. Most experimental studies consider 2D slices of the flame front and a comparison of 2D measurements with representative DNS data has been reported in [13]. The flame front length is typically defined upon identification of a particular isosurface, in analogy to the definition of FSD $\Sigma = \overline{|\nabla c|\delta(c - c^*)}$ based on the fine-grained description [5,14]. The choice of an appropriate species for detecting the flame front (i.e. definition of c and c^*) may give rise to some uncertainties in the flame area evaluation. The focus of this work is to compare flame surface areas

- using an experimental algorithm and a numerical approach
- based on different isosurfaces (i.e. using the fine-grained FSD definition)
- for different species mass fractions
- in three different regimes of combustion

with the corresponding turbulent flame area calculated as the volume integral of Σ_{gen} (see Eq. (5)) in order to quantify possible deviations between experimental and numerical approaches. The flame area analysis will be conducted first for three-dimensional datasets and secondly using two-dimensional cross-sections through the flame. In addition, the validity of Damköhler's first hypothesis will be assessed in three different regimes of combustion and based on different species-specific flame areas. The analysis is based on a detailed chemistry DNS database of turbulent statistically planar flames, which will be described in the next section together with details in regards of the numerical scheme. Results will be discussed in detail in section 4 and finally conclusions will be drawn.

2. DNS DATABASE

A three-dimensional DNS database (Im et al. [15]) of freely-propagating statistically planar turbulent H_2-air premixed flames with $\phi = 0.7$, employing a detailed chemical mechanism (Burke et al. [16]) with 9 species and 19 chemical reactions, is considered here. This choice of stoichiometry is motivated by the fact that these H_2-air premixed flames remain globally thermo-diffusively neutral in that the flame speed is insensitive to stretch [17]. Hence, thermo-diffusive instabilities play a minor role in this work. It also implies that the instances of superadiabatic temperatures are rare in this database and this will not affect the isosurfaces considered in this work ($i.e.\ 0.3 \leq c_T \leq 0.7$). The thermo-physical properties are taken to be temperature dependent and are expressed according to CHEMKIN polynomials. The unburned gas temperature T_0 is taken to be 300K, which yields an unstrained laminar laminar flame speed of $S_L = 135.62\mathrm{cm/s}$ under atmospheric pressure, whereas the adiabatic flame temperature is $1980K$. The inflow values of normalised root-mean-square turbulent velocity fluctuation u'/S_L , turbulent length scale to flame thickness ratio l_T/δ_{th}, Damköhler number $Da = l_T S_L/u'\delta_{th}$, Karlovitz number $Ka = (\rho_0 S_L \delta_{th}/\mu_0)^{0.5}(u'/S_L)^{1.5}(l_T/\delta_{th})^{-0.5}$ and turbulent Reynolds

number $Re_t = \rho_0 u' l_T/\mu_0$ for all cases are presented in Table 1 where μ_0 is the unburned gas viscosity, $\delta_{th} = (T_{ad} - T_0)/\max|\nabla T|_L$ is the thermal flame thickness and the subscript 'L' is used to refer to unstrained laminar flame quantities. The turbulent length scale l_T is the most energetic scale of the Passot-Pouquet spectrum which is used to generate inflow turbulence. It is worth mentioning that the longitudinal integral scale L_{11} is a factor of 2.5 smaller than l_T. The cases investigated in this study are representative of three regimes of combustion: case A: corrugated flamelets (CF, $Ka < 1$), case B: thin reaction zones (TRZ, $1 < Ka < 100$) and case C: broken reaction zones regime (BRZ, $Ka > 100$) (Peters [1]). Figure 1 shows instantaneous views of c_T (temperature based reaction progress variable) isosurfaces for cases A-C. In case A, the c_T-isosurfaces lie close together (i.e. ∇c_T is higher), but their distance varies increasingly from case A to case B to case C. This distinction is indicative of the different combustion regimes. The large-scale wrinkled flame surface observed in case A possibly might be attributed to a flame instability as discussed in Klein et al. [18].

Table 1: List of inflow turbulence parameters

Case	u'/S_L	l_T/δ_{th}	Re_t	Da	Ka
A	0.7	14.0	227	20.0	0.75
B	5	14.0	1623	2.8	14.4
C	14	4.0	1298	0.29	126

The domain size is $20mm \times 10mm \times 10mm$ ($8mm \times 2mm \times 2mm$) in cases A and B (case C) and the domain has been discretised by a uniform Cartesian grid of $512 \times 256 \times 256$ ($1280 \times 320 \times 320$) cells. The grid spacing was determined by the flame resolution, ensuring about 10 grid points across δ_{th}. The long side of the computational domain is taken to align with the mean direction of flame propagation. High order finite-difference (i.e. 8th order central differences for the internal grid points and the order of accuracy gradually decreases to 4th order at the non-periodic boundaries) and Runge-Kutta (low storage 4th order) schemes have been

used for spatial-differentiation and explicit time-advancement respectively. The flame was initialized using a steady laminar flame solution. Turbulent inflow and outflow boundaries are taken in the direction of mean flame propagation and transverse boundaries are taken to be periodic. The nonperiodic boundaries are specified using an improved Navier-Stokes characteristic boundary condition technique [19]. A pseudo-spectral method [20] following the Passot-Pouquet spectrum [21] is used to generate auxiliary divergence-free, homogeneous, isotropic turbulent inflow data. The mean inlet velocity has been changed gradually to match turbulent burning velocity as the simulation progresses. The temporal evolution of flame area has been monitored and the simulations have been run up to the point they can be considered to be statistically stationary. Simulations have been carried out for $1.0t_e, 6.8t_e$ and $6.7t_e$ eddy turnover times (i.e. $t_e = l_T/u'$) for cases A-C respectively.

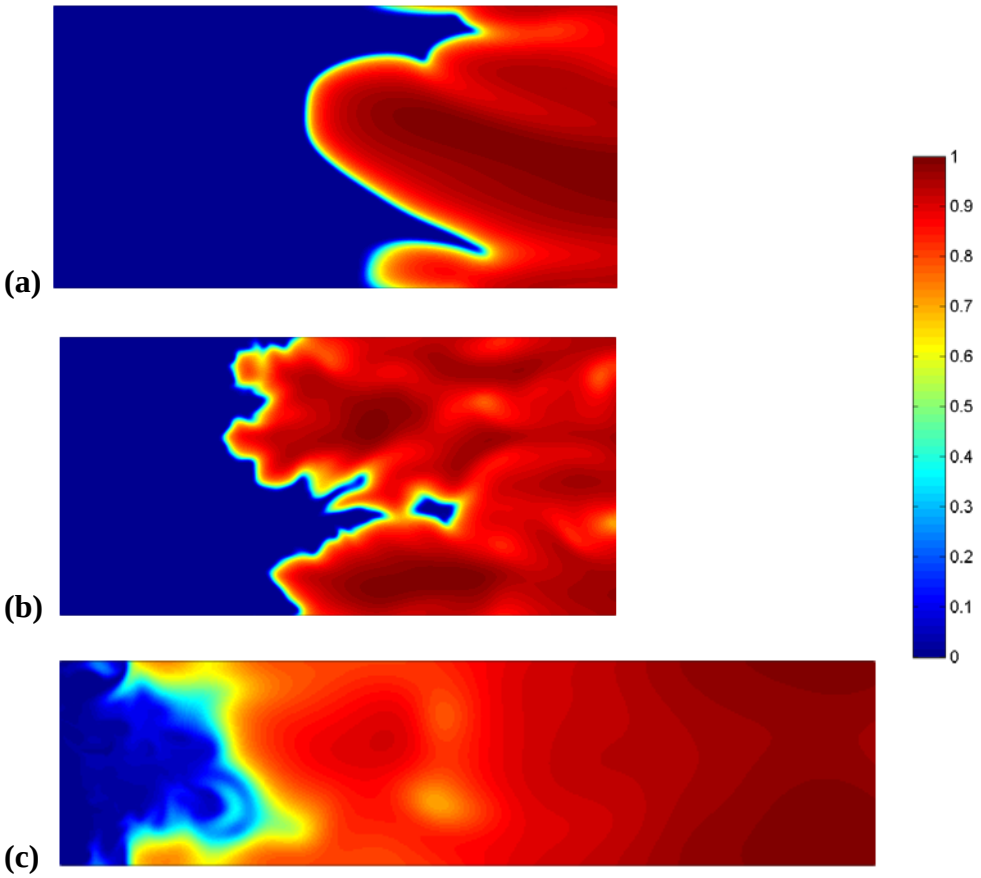

Figure 1. Instantaneous view of c_T isosurfaces for (a)-(c) cases A-C. Note the different scale for case C. The flame burns from right to left here and in the following figures. The cross sectional area has a size of $10 \times 10mm^2$ ($2 \times 2mm^2$) for cases A,B (case C).

The authors confirmed during the original analysis that the results for different time instants after reaching the statistically stationary state are similar to a given time snapshot. Thus, one single snapshot has been considered for the present analysis. As a statistically planar turbulent premixed flame is considered for the current analysis, there are two directions perpendicular to the direction of mean flame propagation, which are statistically homogeneous. This ensures that all evaluations are done over a sufficient number of eddies/flame elements. According to the Ergodic theorem, this is a standard approach in turbulence research and is similar to the practice followed in the existing literature [9,10,13].

3. RESULTS

Turbulent flame areas are intrinsically connected to turbulent burning velocity via Damköhler's first hypothesis. The validity of this hypothesis for the present database is first assessed in the next section. In the remainder of the results section, a detailed analysis of two-dimensional (three-dimensional) flame length (areas) is presented using different methods, different species isosurfaces and different iso-surfaces values.

3.1. Damköhler's first hypothesis

According to Damköhler's first hypothesis, the ratio of normalised burning rate $\Omega = \int_V \dot{w} dV \,/\rho_0 A_L S_L^0 = S_T/S_L^0$ and normalised flame surface area $S = \int_V |\nabla c| dV \,/A_L = A_T/A_L$ given by Ω/S should be unity (see Eqs. 1,5,9). It has been argued that statistically planar flames also experience stretch under turbulent conditions, but, in contrast to flames with mean curvature, the stretch rate dependence nearly disappears upon volume integration for unity Lewis number [7], consistent with the findings in [9,10]. In other words S_L' can, for statistically planar unity Lewis number flames, be approximated as $S_L' \approx S_L^0$. However, this equality becomes invalid in the case of statistically planar flames with global Lewis number larger or

smaller than unity. It has been reported [22] that S_T/S_L^0 can assume values considerably larger than A_T/A_L (i.e. $\Omega/S > 1$) for flames with global Lewis number smaller than unity ($Le \ll 1$). Conversely, $S_T/S_L^0 < A_T/A_L$ (i.e. $\Omega/S < 1$) was found for Lewis numbers larger than unity ($Le > 1$).

Table 2 shows the values of Ω/S where Ω and S are calculated for reaction progress variables based on T, H_2O, O_2, H_2. It can be seen from Table 2 that for a planar flame Eq. (10) remains approximately valid for temperature based reaction progress variable even in the BRZ regime, provided the flame area A_T is calculated as $A_T = \int_V \Sigma_{gen} dV$. Doing the same exercise with major species H_2O and O_2 yields good agreement with Eq. (4) in the CRF and TRZ regime but considerable deviations in the BRZ regime. This possibly might be attributed to Karlovitz number effects, as it has been argued by Peters [1] that curvature effects dominate with increasing Karlovitz number. Finally, the results are less satisfactory for a H_2 based reaction progress variable and it is found that $S_T/S_L > A_T/A_L$ (i.e. $\Omega/S > 1$) in all cases. As hydrogen has a Lewis number considerably smaller than unity this observation is consistent with earlier findings in [22].

Table 2: Normalized burning rate divided by normalized flame area based on $\dot{\omega}_X$ and c_X where $X = T, H_2O, O_2H_2$.

progress variable	Case A Ω/S	Case B Ω/S	Case C Ω/S
T	0.99	1.02	0.94
H_2O	0.98	0.97	0.86
O_2	0.98	0.99	0.84
H_2	1.17	1.30	1.34

The ratio of Ω/S can be approximated in the following manner subject to the validity of a linear extrapolation relation based on Markstein diffusivity:

$$\frac{\int_V \overline{(\rho S_d)}_s \Sigma_{gen} dV}{\rho_0 S_L \int_V \Sigma_{gen} dV} = \frac{\int_V \rho S_d |\nabla c| dV}{\rho_0 S_L \int_V |\nabla c| dV} \approx \frac{\int_V \rho_0 (S_L - 2D_M \kappa_m) |\nabla c| dV}{\rho_0 S_L \int_V |\nabla c| dV}$$
$$= \frac{\rho_0 S_L A_T - 2\int_V \rho_0 D_M \kappa_m |\nabla c| dV}{\rho_0 S_L A_T} = \frac{\rho_0 S_L A_T - 2\rho_0 D_M \langle \kappa_m \rangle_S A_T}{\rho_0 S_L A_T} \quad (11)$$

where D_M denotes the Markstein diffusivity [23], κ_m is the mean curvature of the flame front and $\langle \kappa_m \rangle_s = \int_V \kappa_m |\nabla c| dV / \int_V |\nabla c| dV$ is the global surface-weighted curvature. The expression $\rho S_d \approx \rho_0 S_L - 2\rho_0 D_M \kappa_m$ used in the derivation of Eq. (11) is not strictly correct because D_M is not necessarily constant. However, it is a reasonable assumption, which can be demonstrated in the following manner using the density weighted displacement speed $S_d^* = \rho S_d / \rho_0$ where ρ_0 is the unburned gas density. The density weighted displacement speed S_d^* can be written as: $S_d^* = \rho(S_r + S_n)/\rho_0 + \rho S_t/\rho_0$ where $S_r = \dot{w}/\rho|\nabla c|$, $S_n = \vec{N} \cdot \nabla(\rho D \vec{N} \cdot \nabla c)/\rho|\nabla c|$ and $S_t = -2D\kappa_m$ are the reaction, normal diffusion and tangential diffusion components of displacement speed [1,25-27]. This leads to $S_d^* \approx S_L - 2\rho D/\rho_0 \kappa_m$, subject to the assumption $\rho(S_r + S_n) \approx \rho_0 S_L$ which is reasonable for unity Lewis number flames, as $(S_r + S_n)$ remains weakly correlated with curvature [25-27]. Moreover, ρD is often assumed to be constant [1] and subject to this assumption along with $\rho(S_r + S_n) \approx \rho_0 S_L$ for unity Lewis number flames, one gets: $S_d^* \approx S_L - 2D_0 \kappa_m = S_L - 2D_M \kappa_m$. This suggests that $D_M \approx D_0$ can be reasonably valid once $\rho(S_r + S_n) \approx \rho_0 S_L$ is considered. It is also worth mentioning that analytical expressions of D_M (e.g. $2D_M/D_0 = (1+\tau)\ln(1+\tau)/\tau + 0.5(\beta/\tau)(Le-1)\int_0^\tau \{\ln(1+x)/x\}dx$ with τ, Le and β being the heat release parameter, Lewis number and Zel'dovich number respectively) [2] do not have any dependence on reaction progress variable.

In summary, Eq. (11) reads:

$$\frac{\Omega}{\mathrm{S}} = \frac{S_L'}{S_L} = 1 - \frac{2D_M\langle\kappa_m\rangle_S}{S_L}. \quad (12)$$

This demonstrates, that even for a statistically planar flame (i.e. $\langle\kappa_m\rangle \approx 0$) the validity of Eq. (10) is related to the value of the Markstein diffusivity (depending on the species used for defining the reaction progress variable) and furthermore on the correlation between κ_m and $|\nabla c|$ which affects $\langle\kappa_m\rangle_S$. Although the correction of displacement speed by a linear extrapolation relation involving Markstein diffusivity has limitations [24] as it is known to depend on global Lewis number [25], turbulent Reynolds number [26], flame geometry [27] and chosen isosurfaces value c [28], it is a standard approximation in turbulent premixed combustion modelling [2] and considered useful for a simplified analysis of the governing equations. It is also worth mentioning that the correction of displacement speed by a linear relation involving curvature gave very satisfactory agreement with the DNS data in Ref. [7].

3.2. Challenges in flame area determination based on isosurfaces

After having verified that Eq. (10) is a good approximation for temperature T, H_2O and O_2 based reaction progress variables (for statistically planar flames), it will be important to compare the method for determining flame surface areas which is typically used in DNS with that adopted in post-processing experimental data. The first question to address is the influence of the scalar quantity used for identifying the flame front in experiment.

A linear combination of the mass fractions of product species (e.g. CO, CO_2 and H_2O) is often used for defining reaction progress variable for hydrocarbon-air flames where there can be equilibrium reactions involving these species (e.g. $CO + H_2O \leftrightarrow CO_2 + H_2$ and $CO + \frac{1}{2}O_2 \leftrightarrow CO_2$) [29]. This does not apply to H_2 −air flames, as H_2O is the only product species. Further,

experimental studies do not consider such linear combinations but individual species mass fraction for the definition of reaction progress variable. For this reason, the discussion is limited to comparing individual species in this paper.

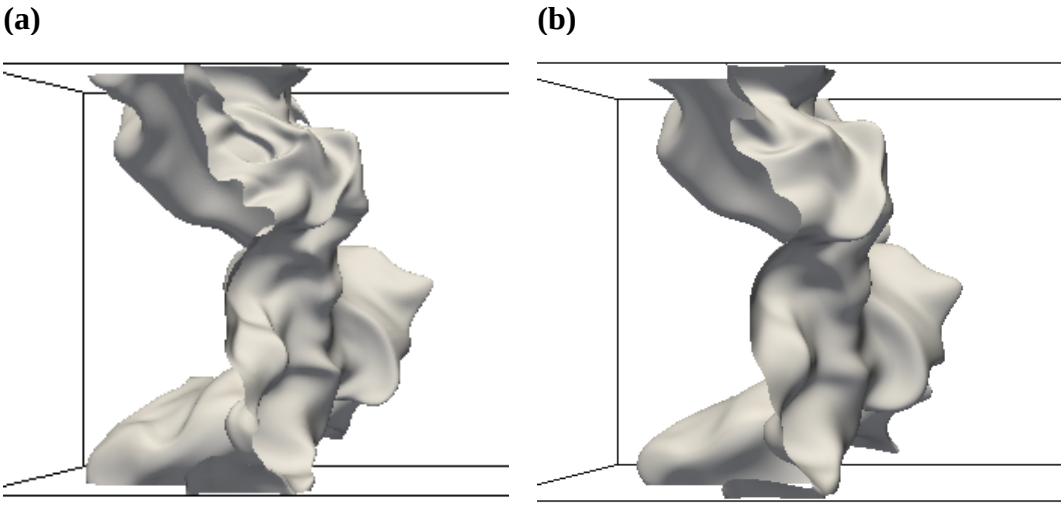

Figure 2. Instantaneous view of (a) $Y_{OH}(c_T = 0.1)$ and (b) $Y_{H2}(c_T = 0.1)$ isosurfaces for case C. Only a part of the domain is shown. The cross sectional area has a dimension of $2 \times 2mm^2$.

Figure 2 depicts the difference in surface area based on isosurfaces of $Y_{OH}(c_T = 0.1)$ and $Y_{H2}(c_T = 0.1)$ for case C. The expression $Y_m(c_T = 0.1)$ is used to indicate the value of Y_m corresponding in a laminar flame to $c_T = 0.1$. It is clearly seen that the hydrogen isosurface is notably less wrinkled, which can partially be attributed to its high diffusivity (see Table 3), but chemical consumption also plays a role.

Table 3: Species diffusivities in the unburned mixture in decreasing order.

Species	$\boldsymbol{H}$	$\boldsymbol{H_2}$	$\boldsymbol{O}$	$\boldsymbol{OH}$
$\frac{D}{10^5}[\frac{m^2}{s}]$	13.6	9.95	3.87	3.80
Species	$\boldsymbol{H_2O}$	$\boldsymbol{HO_2}$	$\boldsymbol{H_2O_2}$	$\boldsymbol{O_2}$
$\frac{D}{10^5}[\frac{m^2}{s}]$	2.72	2.49	2.48	2.41

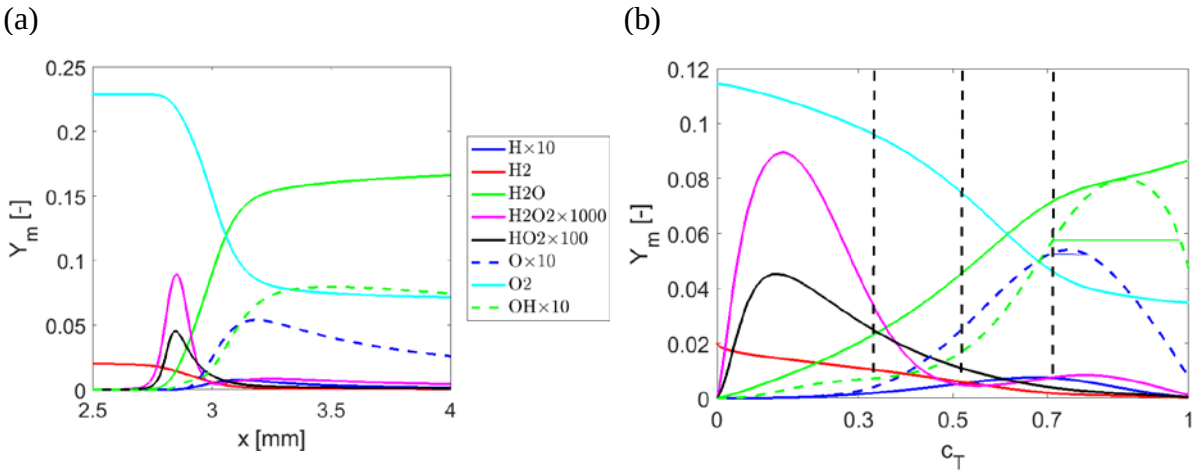

Figure 3. Species mass fractions for the laminar H_2-air flame plotted against (a) flame normal distance x; (b) temperature based reaction progress variable. The horizontal blue and green lines indicate two locations where $Y_O = Y_O(c_T = 0.7)$ and $Y_{OH} = Y_{OH}(c_T = 0.7)$.

Figure 3 (a) shows the different species mass fractions of the laminar hydrogen-air flame plotted as a function of (a) direction of flame propagation and (b) non-dimensional temperature c_T. Three different isosurfaces ($c_T = 0.3, 0.5, 0.7$) have been selected for the subsequent analysis. Higher or lower values of c_T have not been considered due to the possibility of local interaction of the isosurfaces $c_T = 0.1, 0.9$ with the left respectively right boundary of the domain. Besides temperature, which is used in this work, a reaction progress variable can only be defined based on a species mass fraction i.e. major products or reactants (H_2, O_2, H_2O), which exhibits a monotonic trend. If for example c_{O2}=0.3,0.5,0.7 were chosen for this analysis this would have resulted in a slightly narrower range within the flame brush i.e. roughly $0.39 \leq c_T \leq 0.62$ which is

unlikely to change the qualitative nature of this analysis. Finally, it is mentioned, that the maximum reaction rates for the major product or reactant species are found at a value of c_T slightly larger than 0.6, i.e. in the range considered for this analysis. Figure 3 (b) illustrates the problem of non-unique mapping of c_T and Y_m for non-monotonic mass fractions. As an example the mass fractions of OH and O in the laminar flame corresponding to $c_T = 0.7$ can again be found on the burned gas side for $c_T > 0.7$ and this can potentially give rise to considerably larger flame surface area estimates (please refer to the horizontal blue and green line in Fig. 3b). For H_2O_2 there are even four locations corresponding to $Y_{H_2O_2}(c_T = 0.7)$.

Accordingly it is necessary to avoid the species which lead to multiple isosurfaces due to non-unique mapping between c_T and Y_m. This results in large errors of flame area as illustrated in Figure 4 (a) for a H mass fraction corresponding to $c_T = 0.3$. Finally, Fig. 4(b) illustrates modelling challenges in the BRZ regimes where local partially unburned pockets lead to disconnected isosurfaces which represent significant deviations from the flamelet regime.

(a) **(b)**

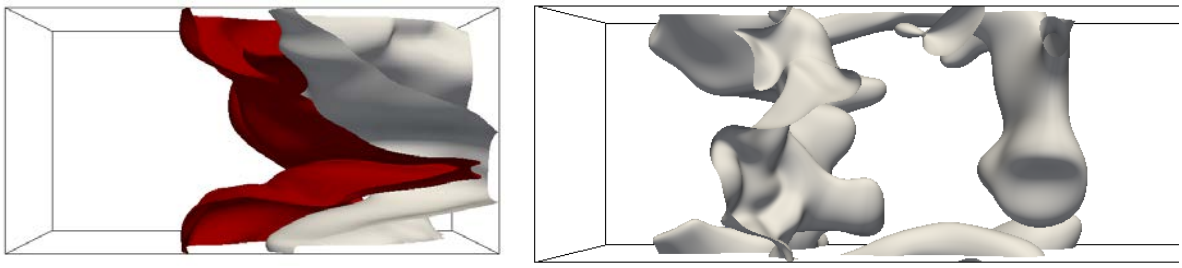

Figure 4. (a) Double $Y_H(c_T = 0.3)$ isosurfaces (in different colours) for case A; (b) Instantaneous view of $Y_{O2}(c_T = 0.7)$ isosurface for case C. The cross sectional area has a size of $10 \times 10mm^2$ ($2 \times 2mm^2$) for subfigure (a) (subfigure (b)).

The main conclusions of these section are: 1.) In the CF and TRZ regimes, it is necessary to be careful with the choice of species leading to multiple isosurfaces due to non-unique mapping between c_T and Y_m. 2) In the BRZ regime, the isosurface area potentially depends on the choice

of the species as well. Furthermore, local deviations from the flamelet structure (e.g. partially unburned pockets) lead to disconnected isosurfaces, which can, depending on the selected isosurfaces value, result in considerable errors when using the isosurfaces based definition of flame surface area. 3.) The flame area evaluation based on the generalised FSD does not depend on a threshold value and is in this sense more robust.

3.3 Sensitivity of flame area evaluation regarding the selection of a particular isosurface

Next, the influence of the isolevel and the scalar quantity selected for evaluation of the flame area will be analysed. Figure 5 shows the ratio of isosurface based turbulent flame area $A_T^{iso} = A_T^{iso}(Y_m)$ and $A_T^{FSD} = A_T^{FSD}(T) = \int_V \Sigma_{gen} dV$ (i.e. normalisation is based on c_T in all cases) for different species and different values of $Y_m(c_T)$.

The ratio of A_T^{iso}/A_T^{FSD} signifies the difference of both methods. Although A_T^{FSD}/A_T^{iso} would work in the same manner, it makes sense to use as reference a method most suitable for postprocessing DNS data. The use of A_T^{FSD} is very common in the modelling of turbulent premixed flames see e.g. [30] and we adopted the same approach here. It is worth mentioning that the flame area calculation based on the volume integral of FSD has several advantages, which are listed below:

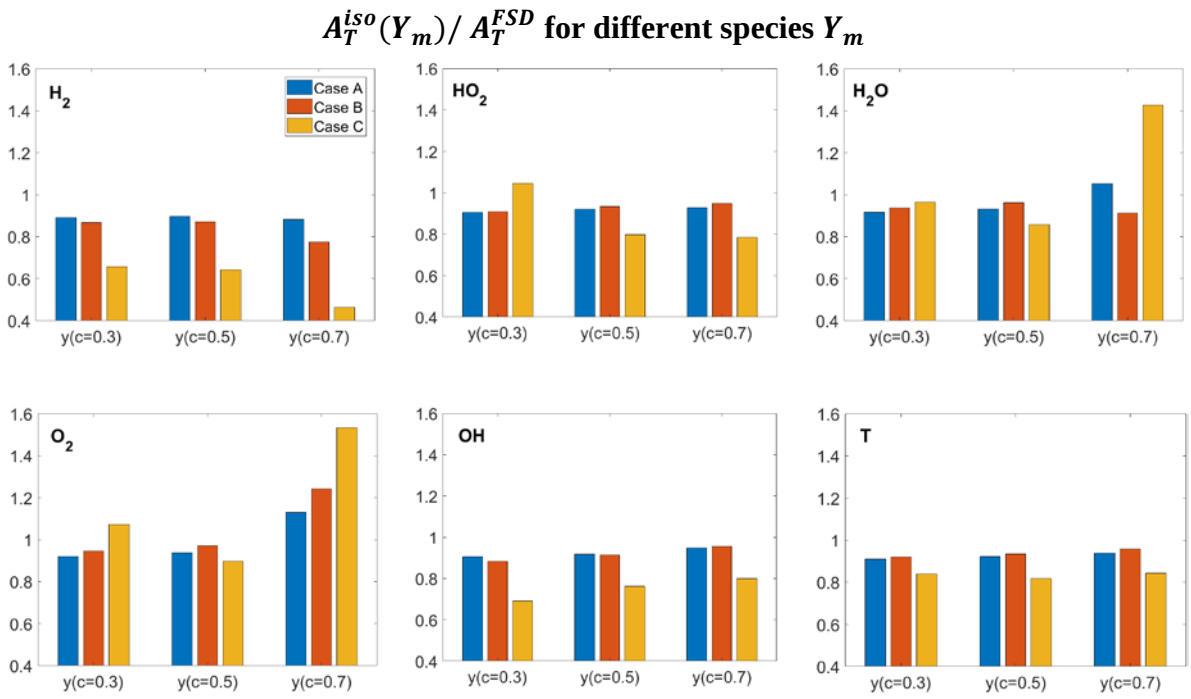

Figure 5. Flame area $A_T^{iso}(Y_m)$ based on three isosurfaces of the mass fractions Y_m corresponding to the isosurfaces $c_T = 0.3, 0.5, 0.7$ for selected species as well as temperature based reaction progress variable c_T for cases A, B, C. All quantities are normalised by A_T^{FSD}, i.e. the volume integrated generalised FSD Σ_{gen} (based on c_T).

1. As $|\nabla c|$ is a field variable, the definition of the generalised FSD and hence A_T^{FSD} is valid irrespective of the value of Karlovitz number [31]. This is in contrast to the flame area based on an isosurface, which implicitly assumes an infinitely thin flame front, which is typical of the corrugated flamelets regime.

2. The definition of turbulent flame area based on generalised FSD is independent of any threshold values again in contrast to the alternative definitions.

3. Damköhler's hypothesis can be derived exactly using A_T^{FSD} (see Eqs. 1-10) based on the first principle in the limit of vanishing stretch (i.e. when the flame speed can be approximated as $S_L = S_L^0$), whereas additional assumptions are required if A_T^{iso} is used.

The quantity A_T^{iso} is evaluated for a given particular isosurface, whereas A_T^{FSD} represents an integral value over the whole flame brush and hence moderate differences between both

quantities should not be unexpected. The area A_T^{iso} (for different species Y_m) in 3D has been determined by a contour based piecewise planar reconstruction using ParaView [32]. The accuracy of this procedure is discussed in the Appendix. The differences observed visually in Fig. 2 can be confirmed from Fig. 5. In fact, the largest under-prediction of flame area A_T^{FSD} based on A_T^{iso} in the BRZ regime can be observed for H_2. Another interesting observation in Fig. 5 is that A_T^{iso}/A_T^{FSD} first decreases slightly for O_2 and H_2O around $c_T = 0.5$ but than increases considerably for $c_T = 0.7$. It can be seen from Fig. 1(c) and Fig. 4(b) that there exists a relatively large partially unburned pocket for case C within the burned mixture. This pocket will immediately result in gradients of temperature and hence A_T^{FSD} increases and consequently A_T^{iso}/A_T^{FSD} decreases for $c_T = 0.5$. This happens because the temperature does locally not reach values as low as $c_T = 0.5$ and hence $A_T^{iso}(Y_m(c_T = 0.5))$ does not get affected. However, the threshold value for $Y_{O2}(c_T = 0.7)$ is attained in this pocket (see Fig. 4 (b)) resulting in a sudden increase of A_T^{iso}. This demonstrates that the flame area evaluation based on Eq. (5) is considerably more robust than other alternatives, in the sense that it does not depend on a threshold value. The above argument serves only for illustration and neglects the possibility of turbulent distortion of the laminar flamelet structure.

The ratio of A_T^{iso}/A_T^{FSD} remains relatively close to, but slightly smaller than unity in the CF and TRZ regimes of combustion. It is important to note that for species mass fractions with non-monotonic c_T dependence, this result could only be achieved by combining the selection of the isosurface with a temperature based threshold function as a second criterion in ParaView. Fig. 5 shows that, depending on the species and the selected isosurface value, differences in A_T^{iso}/A_T^{FSD} of up to 10% can be observed between isosurface based flame area and flame area based on Eq. (5) by volume integrating Σ_{gen}. Especially in the BRZ regime, the latter method (i.e. Eq. (5)) is considerably more robust and differences of more than 40% have been observed

(see Table 2 and Fig. 5). The normalisation by A_T^{FSD} serves as a reference, but A_T^{iso}/A_T^{FSD} should not necessarily be understood as a relative error, as the determination of A_T^{FSD} depends to some extent on the definition of reaction progress variable.

3.4. Two dimensional evaluation of flame length

Although it has been recently demonstrated [33] that spatial and temporal evolution of the 3D flame structure is possible using time-resolved tomographic OH-LIF, experimental evaluation of 3D isosurfaces is not yet standard. Therefore, the analysis of Fig. 5 is repeated for six different 2D slices through the flame and corresponding results for $c_T = 0.3,0.5,0.7$ are shown in Fig. 6. The cross sections are given by three $x-y$ planes with $z/W = 0.25,0.5,0.75$ and three $x-z$ planes with $y/W = 0.25,0.5,0.75$ where W denotes the spanwise width of the computational domain. For the sake of brevity, only one major product (H_2O) is considered here, but results are qualitatively similar for other species. It can be seen from Fig. 6 that depending on how the 2D section cuts the 3D flame surface, one gets a considerable scatter of L_T^{iso}/L_T^{FSD} around unity, where L denotes the flame contour length and evaluation is done in analogy to the 3D case: the length of isosurfaces in 2D has been determined by a contour based piecewise linear reconstruction using ParaView and L_T^{FSD} represents the integral of Σ_{gen}^{2D}, where $|\nabla c|$ is based on the respective 2D gradients. In the CF regime in Case A, the deviations are of the order of $\pm 20\%$ but they increase to $\pm 50\%$ in the TRZ and BRZ regime due to large flame wrinkling across a broad range of scales. In an average sense, the mean value might be roughly correct but largely wrong conclusions can be drawn from instantaneous snapshots. In cases B and C, the mean value L_T^{iso}/L_T^{FSD} tends to be slightly smaller (larger) than unity towards the fresh (burned) gas side.

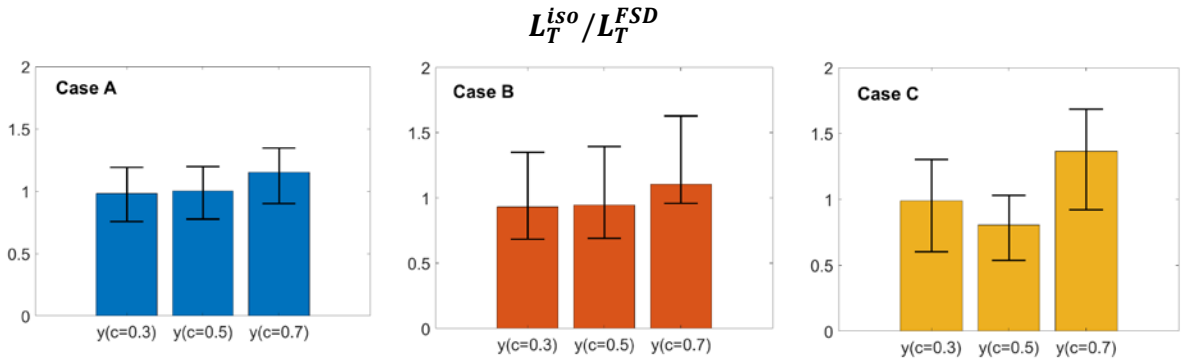

Figure 6. Normalised, H_2O mass fraction based, flame length determined in ParaView, for three different isosurfaces and six different cross sections. The bars represents the average from six different 2D cross sections; the errorbars represent the minimum and maximum value over all samples. Quantities are normalised by the integrated generalised two dimensional FSD Σ_{gen}^{2D}.

3.5. Evaluation of an algorithm designed for experimental determination of flame length

While determining the isosurface of a particular scalar quantity (or alternatively the FSD) is straightforward based on DNS data, this does not hold true for experimental data. Typically, several steps of image processing are used to reduce noise and to extract the flame front. Because of the different nature of the data, different algorithms are used for postprocessing DNS and experimental data and it will be of interest to compare both approaches. Hence, the 2D analysis has been repeated and results are shown in Fig. 7 where, instead of using L_T^{iso}, the flame length is determined based on a procedure for postprocessing experimental data [34,35] and the result will be denoted by L_T^{exp}. The flame front has been detected using a Canny-Edge filter [36]. The FSD is subsequently calculated following Donbar et al. [34] where FSD is defined as $\lim_{\Delta x \to 0} L_{cell}/\Delta x^2$ and L_{cell} is the average flame front length in a square control area with edge length Δx. Finally, in the context of this work, the flame length is obtained by integration of FSD. Donbar et al. [34] suggested to determine flame length based on a binning (interrogation box) size Δ_B (i.e. Δx is replaced by Δ_B), which should be selected in a range between the reaction zone thickness δ_R and the turbulent flame brush thickness δ_T (i.e. $\delta_R \ll \Delta_B \ll \delta_T$) in order to obtain converged results which are independent of Δx. As the correct

parameter Δ_B is a-priori unknown, results in Fig. 7 are shown for a range of binning sizes ranging from $\Delta_B = 0.2\delta_{th}$ up to $\Delta_B = 9.0\delta_{th}$. Due to the lack of a precise anchoring mechanism in turbulent planar flames, the turbulent flame brush thickness is difficult to determine, but for reference it is mentioned that $9\delta_{th}$ correspond roughly to 16% (40%) of the domain length for cases A,B (case C). Again, for the sake of brevity, results are shown only for H_2O mass fraction. Nevertheless, it has been checked for species H_2, O_2, OH that results are qualitatively similar. Figure 7 shows that L_T^{exp}/L_T^{FSD} approaches unity with increasing binning size but a fully converged state is not achieved except for case C. The ratio L_T^{exp}/L_T^{FSD} tends to be larger than unity for case A, around unity for case B and smaller than unity for case C.

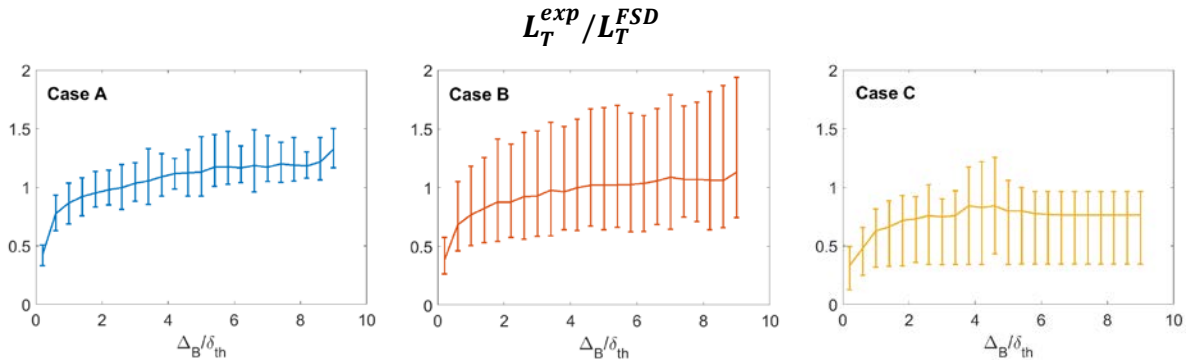

Figure 7. Normalised, H_2O mass fraction based, flame length determined based on a procedure for postprocessing experimental data [34,35], plotted against the bin size, which is given in multiples of the thermal flame thickness δ_{th}=0.354mm. The line represents the average from six different 2D cross sections, the bars represent the minimum and maximum value. Quantities are normalised by the integrated generalised two dimensional FSD Σ_{gen}^{2D} (based on c_T).

Similar to Fig. 6, six different cross-sections are considered. The scatter is around 20% for case A but considerably larger for cases B and C. In a real comparison between DNS and experimental data, it is likely that experimental noise would introduce additional discrepancies.

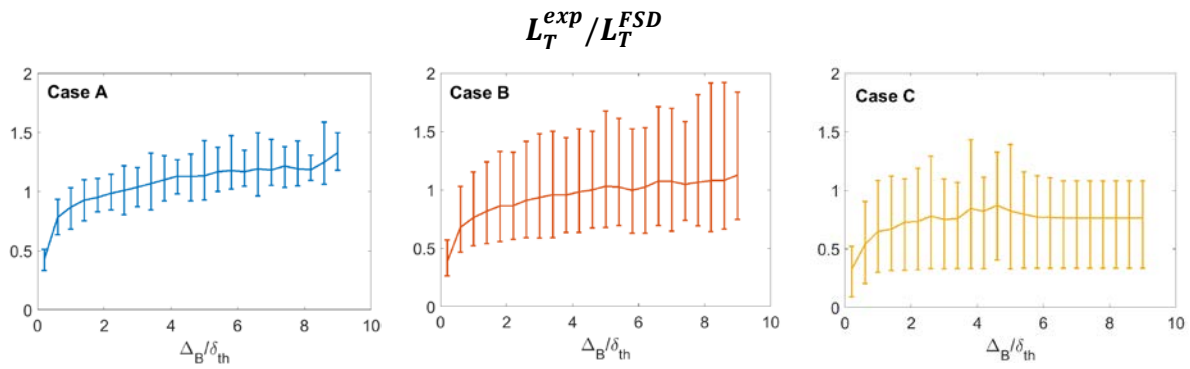

Figure 8. Refer to caption of Fig. 7. Here, before postprocessing data has been filtered with a filter size of 100 μm.

It is worth noting that the fluctuations of mean L_T^{exp}/L_T^{FSD} (i.e. the solid lines) with respect to binning size are rather small in Fig. 7. The flame surface area determination according to Donbar et al. [34] depends on the probability of finding the flame in the interrogation box, clearly showing that this is a question of statistics and hence minor fluctuations should be expected. Qualitatively similar variability of L_T^{exp} has been reported in Donbar et al. [34].

Finally, it is worth mentioning that the DNS resolution in particular for case C is higher compared to what can be achieved in laser diagnostics of combustion applications, where the in-plane resolution is typically of the order of 100 μm [37] but can also be smaller [38], and the out-of-plane resolution is usually larger. In order to account for this effect, the DNS data has been filtered with a filter size of 100 μm. For cases A and B (case C), this corresponds roughly to $2.5\Delta_{DNS}$ ($15\Delta_{DNS}$). The results in Fig. 8 indicate that results do not change considerably in comparison to Fig. 7.

3.6. Implications of 2D versus 3D measurements

It is often difficult to carry out three-dimensional measurements of scalar gradient magnitude in order to determine FSD. However, two-dimensional measurements neglect the flame curvature in the third direction and hence underestimate flame wrinkling and flame surface area

based on extrapolated two-dimensional FSD measurements. Based on the assumption of isotropy of the angle between the local flame normal and the normal vector of the measurement plane a correction factor of $4/\pi$ was derived in [39,40]. The implications of two-dimensional measurements will be discussed in this last section. The magnitude of the two-dimensional projection of the actual gradient of reaction progress variable is evaluated here using the instantaneous lateral and axial gradients of c_T according to the following definition:

$$A_T^{FSD,tt} = \int_V \sqrt{\left(\frac{\partial c}{\partial y}\right)^2 + \left(\frac{\partial c}{\partial z}\right)^2}\, dV$$

$$A_T^{FSD,nt} = \int_V \frac{1}{2}\left[\sqrt{\left(\frac{\partial c}{\partial x}\right)^2 + \left(\frac{\partial c}{\partial y}\right)^2} + \sqrt{\left(\frac{\partial c}{\partial x}\right)^2 + \left(\frac{\partial c}{\partial z}\right)^2}\right] dV \tag{13}$$

$$A_T^{FSD,2D} = \frac{1}{3}\left(2A_T^{FSD,nt} + A_T^{FSD,tt}\right)$$

where indices t, n denote the direction tangential and normal to mean flame propagation. A similar methodology has been used by Hult et al. [13] according to the following logic: In 3D generalised FSD is defined as $\Sigma_{gen} = |\nabla c| = \sqrt{\left(\frac{\partial c}{\partial x}\right)^2 + \left(\frac{\partial c}{\partial y}\right)^2 + \left(\frac{\partial c}{\partial z}\right)^2}$. If only two dimensional measurements are available they can be arranged in a plane normal to flame propagation by using gradients of c in y and z direction. This gives rise to $A_T^{FSD,tt}$ by using a two dimensional definition of Σ_{gen} in the following manner: $\sqrt{\left(\frac{\partial c}{\partial y}\right)^2 + \left(\frac{\partial c}{\partial z}\right)^2}$. If the observation plane is parallel to mean flame propagation direction the evaluation of FSD can exemplarily be done by using gradients in $x - y$ or $x - z$ planes. Due to rotational symmetry both methods are used and the mean value is calculated. This gives rise to $A_T^{FSD,nt}$ and $A_T^{FSD,2D}$ represents the average using all 3 measurement planes.

Figure 9 shows that the absence of the gradient in the third direction clearly reduces the magnitude of $A_T^{FSD,nt}$ and $A_T^{FSD,tt}$ in comparison to A_T^{FSD}. It is also obvious that $A_T^{FSD,tt} > A_T^{FSD,nt}$ which demonstrates that measurements of FSD in different perpendicular cross-sections can differ considerably. After averaging the FSD values in the three different measurement sections and correcting them with the factor $4/\pi$, the estimated flame area $4/\pi A_T^{FSD,2D}$ approximates A_T^{FSD} from 3D measurements very closely. Despite this good agreement it is worth mentioning that the correction factor is derived under the condition of isotropy of the angle between the local flame normal and the normal vector of the measurement plane.

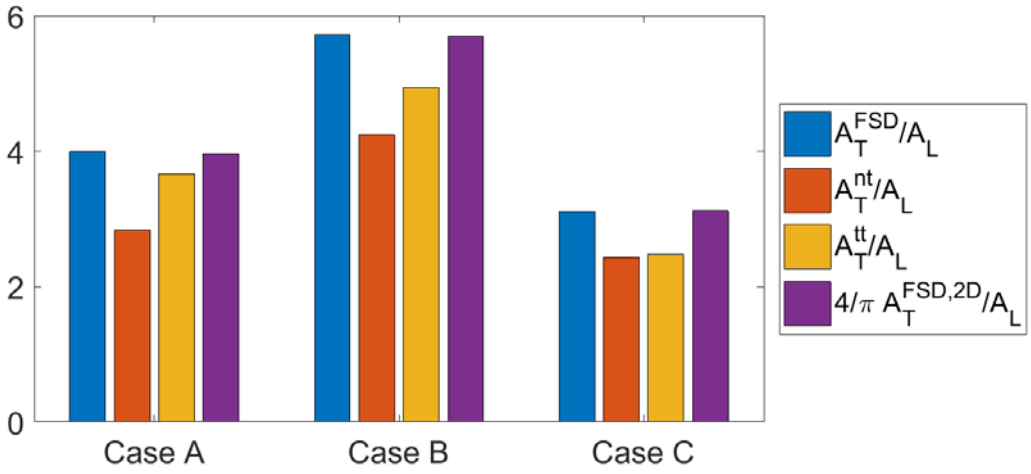

Figure 9. Turbulent flame area normalised by projected flame area A_L, based on volume integration of 3D gradients A_T^{FSD}, 2D gradients A_T^{nt}, A_T^{tt} and an averaged version of 2D gradients corrected by the factor $4/\pi$: $(2 \cdot A_T^{nt} + A_T^{tt})/3 \cdot 4/\pi$.

4. CONCLUSIONS

Flame areas of three freely propagating statistically planar H_2-air flames with an equivalence ratio of 0.7 have been analysed based on a DNS database spanning the CF, TRZ and BRZ regimes of turbulent premixed combustion. The sensitivity of flame area calculation based on different isosurface values for different scalar quantities (i.e. species mass fraction or temperature) has been compared with flame area based on volume integration of the generalised

FSD. Differences of about 10% have been observed depending on the scalar quantity and the isosurface under consideration in the CF and TRZ regimes. In the BRZ regime, the flamelet assumption (i.e. an infinitely thin flame front that allows unique definition of flame area based on a given isosurface) is not strictly valid and as a result the evaluation of flame area based on the fine-grained FSD (i.e. based on isosurfaces) is not robust. Consistent with the observations in Nivarti and Cant [9], it has been found that Damköhler's first hypothesis remains approximately valid, even in the BRZ regime, provided the flame has no mean curvature and the flame area evaluation is based on generalized FSD using temperature for defining reaction progress variable. A comparison of two methods usually used for evaluating flame areas in experiments and DNS revealed that the differences between isosurface based flame area evaluation and FSD based flame area are amplified for two-dimensional measurements. Further, the experimental postprocessing revealed some sensitivity in terms of the interrogation box size. However, by averaging over many two-dimensional sections and by carefully choosing the parameters of the algorithm the differences can be reduced to a satisfactory level.

APPENDIX

The Software Paraview has been used for postprocessing the isosurfaces based flame surface areas [32]. In this respect, piecewise planar interface reconstructions (more precisely a triangulation) have been employed. The very famous "Marching cube" algorithm [41] has been used in order to calculate the isosurfaces. The evaluation of surface areas for our application has been verified in the following manner: The DNS data fields specified in the paper have been filtered and subsequently sampled on grids coarsened by a factor of 2 and 4 in each direction (denoted as DNS2 and DNS4, respectively). The DNS resolution is used as a

reference and the relative errors have been calculated and are reported in the Table 4 below. Results indicate that a sufficiently small error is obtained for all cases. Furthermore, as the grid is coarsened by a factor two and four respectively, it demonstrates nearly quadratic convergence of flame areas with increasing resolution (except for case C).

Table 4: Relative error in % for isosurface based flame area determination ($c_T = 0.5$) using Paraview for cases A,B,C. DNS2 and DNS4 refer to the DNS solution filtered and sampled on a two respectively four times coarser grid.

	Case A	**Case B**	**Case C**
$100 \cdot \frac{\mathrm{DNS} - \mathrm{DNS2}}{\mathrm{DNS}}$	0,86	1,38	1,00
$100 \cdot \frac{\mathrm{DNS} - \mathrm{DNS4}}{\mathrm{DNS}}$	2,91	5,07	3,05

ETHICS STATEMENT

This work did not involve any active collection of human data

COMPETING INTERESTS STATEMENT

We have no competing interests.

FUNDING

The authors are grateful to EPSRC, UK, the German Research Foundation (DFG, KL1456/5-1; DFG 237267381 – TRR 150) and competitive research funding from King Abdullah University of Science and Technology (KAUST) for financial support. Computational support by ARCHER, Rocket HPC, KAUST Supercomputing Laboratory is also gratefully acknowledged.

REFERENCES

[1] Peters N., Turbulent Combustion, Cambridge University Press, (2000).

[2] Poinsot T. and Veynante D., Theoretical and Numerical Combustion, R T Edwards, (2005).

[3] Creta F. and Matalon M., Propagation of wrinkled turbulent flames in the context of hydrodynamic theory, *J. Fluid Mech.*, 680, 225–264, (2011).

[4] Fogla N., Creta F. and Matalon M., The turbulent flame speed for low-to-moderate turbulence intensities: Hydrodynamic theory vs. experiments, *Combustion and Flame*, 175, 155–169, (2017).

[5] M. Boger, D. Veynante, H. Boughanem, and A. Trouvé, Direct numerical simulation analysis of flame surface density concept for large eddy simulation of turbulent premixed combustion, Proc. Combust. Inst. 27, 917–925, (1998).

[6] Driscoll J.F., Turbulent premixed combustion: Flamelet structure and its effect on turbulent burning velocities, Prog. Energy and Combust. Sci., 34, 91–134, (2008).

[7] Chakraborty, N., Alwazzan, D., Klein, M., Cant, R.S., On the validity of Damköhler's first hypothesis in turbulent Bunsen burner flames: A computational analysis, Proc. Combust. Inst., 37 (2018).

[8] Hawkes, E.R., and Cant, R.S., Implications of a flame surface density approach to large eddy simulation of premixed turbulent combustion. Combust. Flame, 126(3), 1617–1629. doi: 590 10.1016/S0010-2180(01)00273-5, (2001).

[9] Nivarti G., Cant S., Direct Numerical Simulation of the bending effect in turbulent premixed flames Proc. Combust. Inst., 36. 1903-1910, (2017).

[10] Ahmed, U., Chakraborty, N. and Klein, M., Insights into the Bending Effect in Premixed Turbulent Combustion Using the Flame Surface Density Transport, Combust. Sci. Technol., accepted, (2019).

[11] Gülder O., Contribution of small scale turbulence to burning velocity of flamelets in the thin reaction zone regime, Proc. Combust. Inst., 31, 1369-1375, (2007).

[12] Sabelnikov V.A., Yu R. and Lipatnikov A. N., Thin reaction zones in constant-density turbulent flows at low Damköhler numbers: Theory and simulations, Phys. Fluids 31, 055104 (2019).

[13] Hult, J., Gashi, S., Chakraborty, N., Klein, M., Jenkins, K.W., Cant, S., and Kaminski, C., Measurement of flame surface density for turbulent premixed flames using PLIF and DNS. Proc. Comb. Inst., 31:1319-1326, 2007.

[14] Pope, S.B., The evolution of surfaces in turbulence, Int. J. Engng. Sci., 26, 445-469, (1988).

[15] Im H.G., Arias P.G., Chaudhuri S., Uranakara H.A., Direct Numerical Simulations of Statistically Stationary turbulent Premixed Flames, 10th Asia-Pacific Conference on Combustion, Topical Review, July 19-22, Beijing, China, (2015).

[16] Burke M. P., Chaos M., Ju Y., Dryer F.L., Klippenstein S.J., Comprehensive H2-O2 kinetic model for high-pressure combustion, I. J. Chem. Kin., 444-472, (2012).

[17] Im H.G. and Chen J.H., Preferential diffusion effects on the burning rate of interacting turbulent premixed hydrogen-air flames, Combust. Flame, 126, 246, (2002).

[18] M. Klein, N. Chakraborty, and S. Ketterl, A comparison of strategies for direct numerical simulation of turbulence chemistry interaction in generic planar turbulent premixed flames, Flow Turb. Combust. (2017) DOI:10.1007/s10494-017-9843-9.

[19] Yoo C. S., Wang, Y., Trouve A. and Im, H. G., Characteristic boundary conditions for direct simulations of turbulent counterflow flames, Combust. Theor. Model. 9, 617 (2005).

[20] Rogallo, R. S., Numerical experiments in homogeneous turbulence, NASA Ames Research Center Report No. 81315, (1981).

[21] Passot T. and Pouquet P., Numerical simulation of compressible homogeneous flows in the turbulent regime, J. Fluid Mech. 181, 441 (1987).

[22] Chakraborty, N., Wang, L., and Klein, M., Streamline segment statistics of premixed flames with non-unity lewis numbers. Physical Review E, E89:033015, (2014).

[23] Chaudhuri, S., Wu, F. and Law C.K., Scaling of turbulent flame speed for expanding flames with Markstein diffusion considerations, Physical Review E, 88 (2013) 033005.

[24] Wu F., Liang W., Chen Z. and Ju Y., Chung K. Law, Uncertainty in stretch extrapolation of laminar flame speed from expanding spherical flames, Proc. Combust. Inst., 35, 663–670, (2015).

[25] Chakraborty, N. and Klein, M., Influence of Lewis number on the surface density function transport in the thin reaction zones regime for turbulent premixed flames. Physics of Fluids, 20, 065102, (2008).

[26] Chakraborty, N., Klein, M. and Cant, S., Effects of turbulent Reynolds number on the displacement speed statistics in the thin reaction zones regime of turbulent premixed combustion. Journal of Combustion, doi:10.1155/2011/473679, (2011).

[27] Klein M., Chakraborty N., Jenkins K.W. and Cant R.S., Effects of initial radius on the propagation of premixed flame kernels in a turbulent environment, Physics of Fluids, 18, 055102, 2006.

[28] Giannakopoulos G.K., Gatzoulis A., Frouzakis C.E., Matalon M., Tomboulides A.G., Consistent definitions of “Flame Displacement Speed” and “Markstein Length” for premixed flame propagation, Combustion and Flame, Combust. Flame, 162, 1249-1264, (2015).

[29] Sandeep A., Proch F., Kempf A.M. and Chakraborty N., Statistics of strain rates and surface density function in a flame-resolved high-fidelity simulation of a turbulent premixed bluff body burner, Phys. Fluids, 30, 065101, (2018).

[30] Haworth, D.C., Applications of turbulent combustion modelling, Turbulent Combustion, Lecture Series 2003-04, von Karman Institute for Fluid Dynamics, March 17-21, (2003).

[31] Chakraborty N. and Klein M., A priori direct numerical simulation assessment of algebraic flame surface density models for turbulent premixed flames in the context of large eddy simulation. Fluids, 20, 065102, (2008).

[32] Utkarsh A., The ParaView Guide: A Parallel Visualization Application, Kitware, ISBN 978-1930934306, (2015).

[33] Pareja, J. , Johchi, A., Li, T., Dreizler, A., Böhm, B., A study of the spatial and temporal evolution of auto-ignition kernels using time-resolved tomographic OH-LIF, Proc. Combust. Inst., 37, 1321-1328, (2019).

[34] Donbar J.M., Driscoll J.F., Carter C.D., Reaction Zone Structure in Turbulent Non-premixed Jet Flames from CH-OH PLIF Images, Combust. Flame 122, 1–19, (2000).

[35] Jainski C., Rißmann M., Böhm B., Dreizler A., Experimental investigation of flame surface density and mean reaction rate during flame–wall interaction, Proceedings of the Combustion Institute 36, 1827–1834, (2017).

[36] Canny, J., A Computational Approach to Edge Detection, Readings in Computer Vision, Morgan Kaufmann Publishers, 184-203, (1987).

[37] Jainski C., Rißmann M., Böhm B., Janicka, J. and Dreizler A., Sidewall quenching of atmospheric laminar premixed flames studied by laser-based diagnostics. Combustion and Flame 183, 271–282, (2017).

[38] Peterson B., Baum E., Böhm B. and Dreizler A., Early flame propagation in a spark-ignition engine measured with quasi 4D-diagnostics, Proceedings of the Combustion Institute, 35, 3829–3837, (2015).

[39] Hawkes, E.R., Sankaran, R., Chen, J.H., Estimates of the three-dimensional flame surface density and every term in its transport equation from two-dimensional measurements, Proc. Combust. Inst., 33, 1447–1454, (2011).

[40] Chakraborty, N., Hawkes, E.R., Determination of 3D flame surface density variables from 2D measurements: Validation using direct numerical simulation, Phys. Fluids 23, 065113, (2011).

[41] Lorensen W.E., Cline H.E., Marching Cubes: A high resolution 3D surface construction algorithm, Computer Graphics, 21, 163–169, (1987).